Quantum efficiency stability of silicon photodiodes

Raj Korde and Jon Geist

The stability of the quantum efficiency of inversion layer, phosphorus-diffused (n on p), and boron-diffused (p on n) photodiodes has been investigated. Unsatisfactory silicon–silicon dioxide interfaces, latent recombination centers in the diffused layers, and moisture absorption by the device were identified as possible causes of instability. Diodes were fabricated using processes in which these sources of instability were carefully controlled. The resulting diodes were subjected to various accelerated aging tests, and the external quantum efficiency of the diodes was monitored during the tests. Diodes made by older procedures, in which some important parameters affecting stability were not controlled, were included in the study for comparison. The major result of this work is the demonstration that n on p photodiodes are inherently more stable than p on n types in the ultraviolet and blue spectral regions, but that stable p on n devices can also be produced with sufficient care.

I. Introduction

Silicon photodiodes are the workhorses for photon detection in the 200–1100-nm spectral region. The most demanding application of silicon photodiodes is in high precision and high accuracy radiometric measurements.[1,2] Despite the importance of a high, stable quantum efficiency to applications of this nature, there is very little information in the literature on the stability of the quantum efficiency of silicon photodiodes.

The susceptibility of the oxide–silicon interface to high levels of UV radiation has been known at least since 1966,[3] yet the few studies of the effect of UV radiation on silicon photodiodes have examined only one aspect of instability, and on an obsolete type of diode.[4–6] And, although concern over the stability of silicon diodes representing the current state of the art was expressed a few years ago,[7] it is only within the last two years that quantitative data on a few commercial devices have been reported.[8–10] These references report that some boron-diffused devices were found to suffer as much as a 10% per year loss of quantum efficiency at 400 nm over a period of a few years of storage. However, none of these authors discusses the details of the mechanisms responsible for the loss of quantum efficiency.

In this paper, we compare the changes in quantum efficiency that were observed in specially fabricated photodiodes when subjected to intense ultraviolet radiation, and storage at high humidity and/or high temperature in an attempt to accelerate the types of instability encountered during the normal use and storage of silicon photodiodes. We specifically ignore oxide stress[11–14] during the application of oxide bias[15] as a source of instability, because it is associated with a particular type of self-calibration[16] procedure and will not be encountered during the normal use and handling of silicon photodiodes. We note that Key *et al.*[12] have shown how to perform the self-calibration with the highest accuracy despite the oxide bias instability, and have pointed out that a diode used for the self-calibration procedure is not a satisfactory shelf standard as a result of the self-calibration. Our concern in this paper is with developing more satisfactory diodes for use as shelf standards, and the spectral regions of interest to us are the UV and short-wavelength visible.

II. Sources of Photodiode Instability

Using published results and our own experience, we have identified a number of possible causes of the loss of short-wavelength quantum efficiency in silicon photodiodes. First let us consider n on p type devices.

It has been proposed and demonstrated that natural inversion layer photodiodes[17] should have a short-wavelength quantum efficiency of 100% due to the nature of the built-in field associated with a strongly inverted layer at the oxide–silicon interface.[18] Instabilities were also encountered with this type of photodiode, but the symptom was not the loss of short-wavelength quantum efficiency, but rather a loss of linearity at the high end of the linearity range. This is what would be expected if the fixed oxide charge that

Raj Korde is with United Detector Technology, Hawthorne, California 90250, and Jon Geist is with U.S. National Bureau of Standards, Gaithersburg, Maryland 20899.

Received 20 June 1987.

induces the inversion layer in the diode were to be neutralized as a result of UV irradiation. Since the inversion layer charge decreases with decreasing oxide charge, the diode inversion layer resistance, which is in series with the diode, would increase. Thus the threshold value of forward bias needed to cause a nonlinearity could be dropped across the increased series resistance by a smaller value of photocurrent, resulting in a loss of linearity range. The opposite effect, an extension of the linearity range by adding charge to the oxide, has been demonstrated.[18]

It has also been proposed that light arsenic or phosphorus doping[19] and the redistribution of the dopant during oxide growth[20] could be used to tailor the built-in field between the oxide–silicon interface and the junction to eliminate recombination at the interface in a manner similar to that occurring with inversion layer diodes,[18] and that such a structure should be resistant to UV irradiation.[19] Indeed, Ref. 19 describes the fabrication of arsenic-doped devices with outstanding resistance to ultraviolet radiation (no change in UV responsivity after 60 days at 20 mW/cm^2). However, sufficient care was not exercised with respect to impurities incorporated into the silicon during and following the prediffusion used to prepare the diodes for arsenic drive-in, and later testing showed a 6.2% decrease in quantum efficiency at 410 nm following baking of the diodes at 110°C for 3000 h. Perhaps, some impurities that were incorporated into the diffused region as latent recombination centers were activated by this treatment, and were able to cause the recombination of a non-negligible fraction of the excess minority carriers created in this region before they could be transported to the junction by the built-in field. The latter conjecture brings us rather naturally to the p on n type of diode, where latent recombination centers in the p type region are well known.

Weizer *et al.*[21] have described metallic impurities, most notably silver, which complex with boron in silicon to form latent recombination centers, and which only become active during the passage of several years. Moisture penetration through the package to the device over a long period of time is also a possible cause of observed changes in the quantum efficiency of boron-diffused devices over extended periods of time. Moisture in conjunction with boron is suspected of causing recombination centers near the oxide–silicon interface,[22] and moisture has been reported to neutralize the ionized boron acceptors by hydrogen injection creating a surface region depleted of ionized boron.[23]

In the latter case, the surface depleted boron ion profile would create a built-in field which moves minority carriers toward the oxide–silicon interface rather than toward the junction. Complementing this effect, the first moisture related effect would increase the number of recombination centers near the oxide–silicon interface, and the second would increase the time that the minority carriers are in the presence of the recombination centers. In both cases an increase in recombination relative to collection by the junction is expected.

Due to the redistribution of boron during oxide growth, it does not seem possible to tailor the built-in field in such a way that the minority carriers spend a negligible time in the presence of oxide–silicon interface recombination traps. Thus, a trap-free interface seems necessary to eliminate interface recombination at short wavelengths where the photogenerated carriers are created in the vicinity of the interface. Inferior interface structures characterized by interface and silicon bulk traps in the vicinity of the interface,[24] the existence of strained bonds at the interface,[25] the presence of excess H and OH in the oxide,[26] and even excessive boron in the oxide[27] have all been correlated with interface traps and latent interface traps. Presumably all these must be minimized by proper process control to obtain a boron-diffused photodiode with a stable UV quantum efficiency.

In view of the above discussion, it would appear to be easier to fabricate stable 100% internal quantum efficiency silicon photodiodes using n on p processes rather than p on n processes. Nevertheless, we had observed some commerical p on n photodiodes that, while not perfect, had close to 100% internal quantum efficiency and were reasonably stable under UV irradiation. Therefore, we decided to examine the long-term stability of p on n, as well as that of inversion layer and n on p metallurgical junction diodes, and to try to correlate the results with the conditions in which the diodes were fabricated.

Two different classes of photodiodes were included in our study. The first class consisted of photodiodes that were specially fabricated with processes designed to avoid the problems that we had identified as likely causes of the deterioration of quantum efficiency with normal use and storage. The second class consisted of commercially available photodiodes representative of the current state of the art of silicon p on n photodiodes during the period of the study. The latter have near 100% internal quantum efficiency over the entire visible spectral region and have been readily available from a few vendors for a number of years, but may not have been produced with the careful processing that was used for the diodes specially fabricated for this study.

As an aside, we note a very recent claim[28] that "silicon photodiodes have inherently poor quantum efficiencies in the UV region." This claim, which was made in connection with a paper advocating edge illumination of silicon photodiodes, strongly implies that high quantum efficiency photodiodes are not commercially available for the UV. This is incorrect and has been since 1979.[29,30] Building a silicon photodiode with a high ultraviolet quantum efficiency has not been the problem. The problem has been to maintain that high quantum efficiency under ultraviolet irradiation and over periods of years. Nevertheless, high UV quantum efficiency devices that have experienced a significant loss of quantum efficiency due to UV irradiation or the ravages of time still have much higher spectral responsivities than the spectral response of a typical silicon photodiode shown in Fig. 1 of Ref. 28.

III. Experimental

Three-inch diameter, float zone, ⟨111⟩ oriented wafers, mirror polished on one side were used to fabricate photodiodes having 1 cm^2 active area. The boron-diffused devices were fabricated on 10-Ω · cm n-type wafers, and the phosphorus-diffused and inversion layer devices were fabricated on 100-Ω · cm p-type wafers.

Figure 1 shows a schematic diagram of the three structures used. Since UV and blue photons are absorbed in the first few hundred nanometers of silicon, the boron and phosphorus diffusions were kept shallow to minimize the possibility of recombination between the oxide–silicon interface and the junction. The spreading resistance profiles of these diffusions are shown in Fig. 2.

Meticulous care, as described by Ghandhi,[31] was exercised during the wafer processing to achieve a high minority carrier lifetime in the diffused layer. At least in the case of the phosphorus diffusions these efforts were successful, and 100% internal quantum efficiency was achieved as shown in Fig. 3. We take this as an indication not only of a high minority carrier lifetime in the diffused region, but also of sufficient phosphorus pile-up at the oxide–silicon interface to lower the minority carriers concentration at the interface, thereby reducing the probability of recombination at any interface defects that exist there after processing, or that become activated by environmental stress. Spreading resistance measurements cannot detect pile-up, so it is not surprising that none is evident in the phosphorus profile shown in Fig. 2.

Various device fabrication parameters, such as the duration and temperature of the impurity deposition, the nature of the oxidizing drive ambient, and the final low and high temperature annealing steps, were varied to investigate their effect on the stability of the quantum efficiency of fabricated diodes, and the optimum combination was used in fabricating the stable devices reported in this paper. Since these are the steps that proved crucial to controlling stability, they will not be described in detail here. Anyone trying to build similar devices could not be assured of achieving good stability without repeating the optimization process for his own particular fabrication facility, because the temperatures of the various furnaces were not calibrated, and other uncharacterized facility parameters might also be important.

In general, it is perspiration rather than inspiration that perfects the processing with respect to device stability, most of the steps having been adequately explained in Refs. 31–33. Extremely high purity chemicals were used for wafer cleaning. Only 99.999% pure gases were used during high temperature wafer processing. And, TCA (1,1,1-trichloroethane) cleaning of the quartz tubes at high temperatures was adopted to avoid sodium and other metallic impurity contamination during high temperature processing.

A clean oxide process, such as described by Botchek[32] was adopted during the growth of the final silicon dioxide antireflection coating to yield diodes

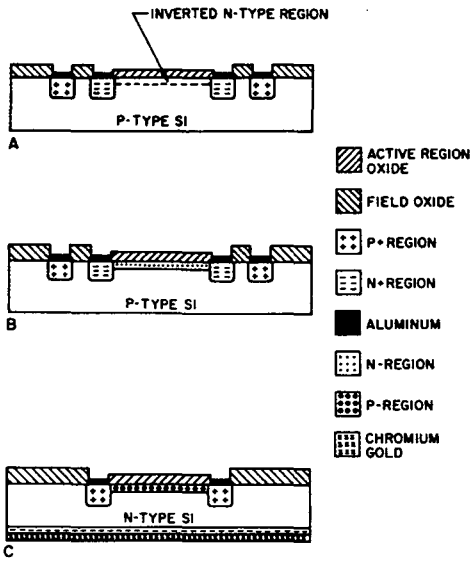

Fig. 1. Schematic diagram of the silicon photodiodes fabricated for this work: (A) inversion layer type; (B) phosphorus-diffused type (n on p); and (C) boron-diffused type (p on n).

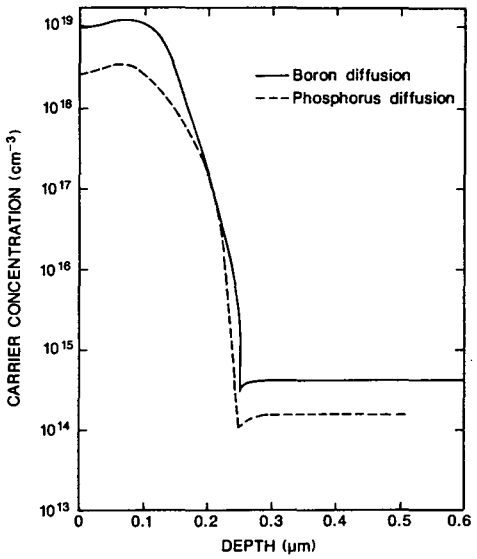

Fig. 2. Spreading resistance profile of boron diffusion in p on n photodiode, and of phosphorus diffusion in n on p photodiode. Phosphorus pile-up at the front interface, if present, is not resolved by spreading resistance measurements.

with very high shunt resistance (100 MΩ at ±10 mV for a 1-cm^2 active area). The devices were then annealed as described by Weinberg *et al.*[33] These steps seem to be necessary to prevent UV-induced charge neutralization in the oxide on inversion layer diodes, as well as to render the oxide–silicon interface less susceptible to UV radiation. Ohmic contacts to the n and p type regions were made by electron beam evaporation of aluminum followed by photolithography to define the contact areas. The wafers were sintered at 450°C for 10 min in pure nitrogen and then sawn into the individual photodiode chips. After the electrical parameters

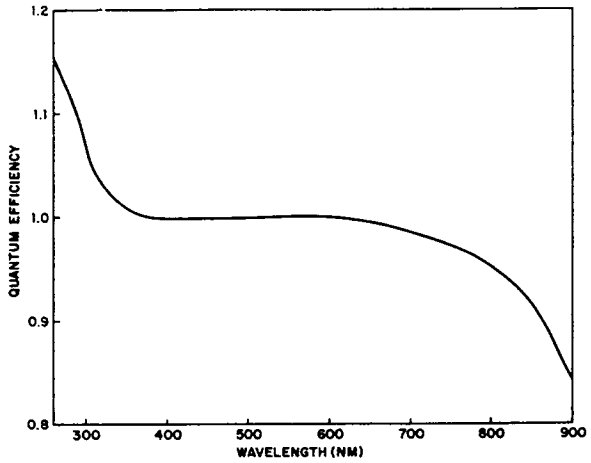

Fig. 3. Internal quantum efficiency as a function of wavelength for phosphorus-diffused diode. The internal quantum efficiency increases above unity at the short wavelengths because more than one electron–hole pair is produced per absorbed photon at these wavelengths as discussed in Refs. 29 and 37.

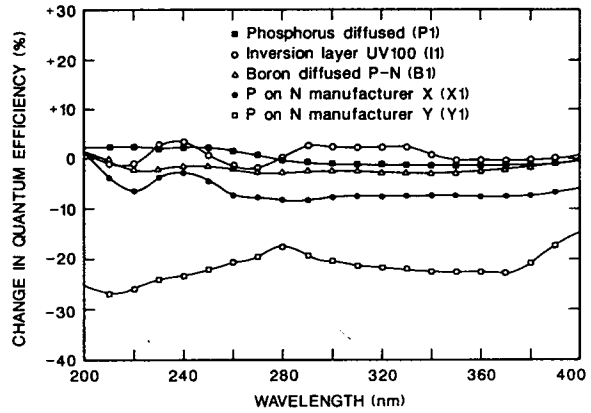

Fig. 4. Relative change in external quantum efficiency as a function of wavelength for silicon photodiodes after exposure to 20 mW/cm^2 of 254-nm radiation for 24 h.

of the chips were tested, they were mounted on the United Detector Technology (UDT)[34] standard BNC package stud using epoxy. The contacts from the *n* and *p* electrodes on the chip to the anode and cathode of the package were made with an ultrasonic wire bonding machine using aluminum wire.

The packages were then sealed with epoxy to a cap having a quartz window. Most of the epoxy used was EPOTEK H77. However, some of the boron-diffused devices were sealed using EPOTEK 731. The former was designed for hermetic seals, and forms bonds whose He diffusion rate is 1×10^{-8} cm^3/s after exposure to 32°C (90°F), 90% RH for 100 h, whereas the latter is not designed for hermetic seals and has not been tested in this way, but it is known that its He outgassing rate would be many orders of magnitude larger in the same conditions.[35]

The external quantum efficiencies of the photodiodes included in this study were measured before and at various times during and after exposure to the accelerated degradation environments. The quantum efficiencies were obtained by spectral response comparison relative to a silicon photodiode standard traceable to the National Bureau of Standards using an *F*4.2, 300-mm focal length, single-grating monochromator with a deuterium arc lamp as a radiation source for the 200–400-nm spectral region, and a quartz–halogen, tungsten filament lamp for the 400–950-nm range. The precision of quantum efficiency transfer measurements using this apparatus is no worse than ±2% of value over most of the 200–950-nm spectral range.

Three different accelerated aging tests were adopted for this study in an attempt to stimulate all possible degradation mechanisms. The first test was exposure of the diode front surface to 20 mW/cm^2 of 254-nm radiation from a low pressure mercury lamp for 24 h. The second test was baking at 100°C for 196 h, and the third was exposure to 37.8°C (100°F), 100% RH for 48 h.

Three *p* on *n* type diodes from other manufacturers were included in the accelerated degradation tests. As far as we know, these diodes (along with the UDT standard process boron-diffused diodes) represented the state of the art in *p* on *n* silicon photodiode stability at the time of this study, but the details of their fabrication and mounting are unknown. Therefore the results for the latter diodes are included only to provide a frame of reference.

IV. Results and Discussion

Figure 4 shows the relative change in the responsivity over the 200–400-nm spectral range of several representative photodiodes after their exposure to 24 h of 20 mW/cm^2 of 254-nm radiation. Before exposure, all these devices, except that from manufacturer X, had nearly 100% collection of the photogenerated carriers created by photons in the 200–550-nm spectral range, with a nominal spectra responsivity at 254 nm of ~0.11 A/W. The initial spectral responsivity of the diode from manufacturer X was 0.09 A/W.

It is evident from Fig. 4 that the inversion layer diodes, the phosphorus-diffused diodes, and the boron-diffused diodes that were specially fabricated for this study show little or no degradation in quantum efficiency after UV exposure. The considerable reduction in quantum efficiency of the other two diodes is probably caused by some combination of an inferior Si–SiO_2 interface,[24] the presence of excessive H and OH bonds,[25,26] and boron[27] in the oxide.

When the final oxide antireflection coating for any of the three types of diode was grown in either dry, impure oxygen, or wet, but otherwise pure, oxygen without the rigorous process control alluded to earlier in this paper, decreases in the 254-nm quantum efficiency of the diodes that were as large as 60% in some cases were observed following exposure to 20 mW/cm^2 of 254-nm radiation for 24 h. Apparently, the final oxide, which serves both as an antireflection coating and the interface passivation, must be an MOS grade SiO_2 coating that is grown using a clean, dry oxide

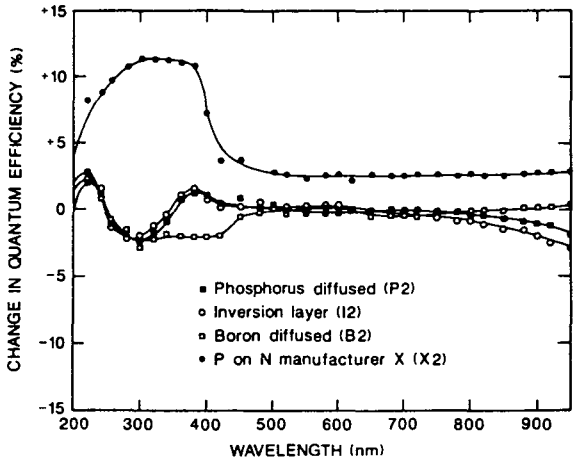

Fig. 5. Relative change in external quantum efficiency as a function of wavelength for silicon photodiodes after exposure to 100°C for 196 h.

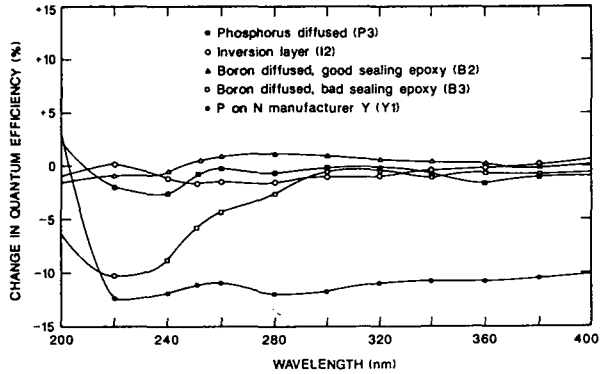

Fig. 6. Relative change in external quantum efficiency as a function of wavelength for silicon photodiodes after exposure to 37.8°C, 100% RH for 48 h.

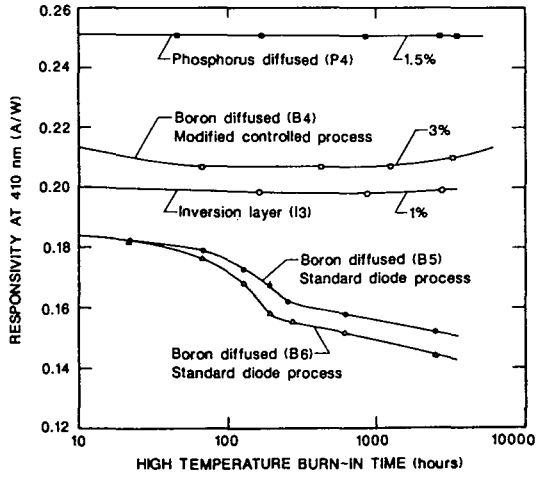

Fig. 7. Change in spectral responsivity at 400 nm as a function of duration of exposure to 110°C.

process including a proper annealing step to assure stability against UV exposure.

Figure 5 shows the change in quantum efficiency over the 200–950-nm spectral range of several representative photodiodes after baking at 100°C for 196 h. We do not know what caused the wavy nature of the curves for photodiodes *P*2, *B*2, and *I*2 between 200 and 300 nm, but it could be a small change in oxide thickness. We imagine that the increase in responsivity of the *p* on *n* device from manufacturer X is a result of moisture outgassing during baking. Indeed, the responsivity of this device was found to return to its original value following exposure to 100% relative humidity at 37.8°C.

Figure 6 shows the change in quantum efficiency of representative photodiodes over the 200–400-nm spectral range following baking at 100% RH, 37.8°C for 48 h. Little or no change is evident in the case of the phosphorus-diffused diode, the inversion layer diode, and one of the boron-diffused diodes (*B*2) fabricated by the new procedure. On the other hand, drastic reductions in responsivity were observed for the other boron-diffused device made by the new procedure (*B*3), and for the *p* on *n* device made by manufacturer Y. Although the boron-diffused devices *B*2 and *B*3 were from the same fabrication lot, they were sealed into their packages using different epoxies. EPOTEK H77, a high hermeticity epoxy, was used for *B*2, while EPOTEK 731, a poorer hermeticity epoxy, was used for *B*3. Therefore, we conclude that it is necessary to provide a moisture-proof seal, either with the proper type of epoxy or the proper type of weld, to prevent a moisture-induced loss of short-wavelength quantum efficiency in *p* on *n* silicon photodiodes.

To investigate their long-term stability, some of the photodiodes were baked for several months at 110°C. They were periodically removed from the oven, allowed to reach ambient temperature, measured at 400 nm, and returned to the oven. Figure 7 illustrates the results of this experiment. Once again, little or no change was observed in the case of the phosphorus-diffused and inversion layer devices, while the boron-diffused device fabricated following the new, better controlled procedure showed only a marginal responsivity change. On the other hand, the boron-diffused devices fabricated using the old standard process, where no efforts were made to control metallic impurity contamination, exhibited a monotonic decrease in responsivity during the prolonged baking. This decrease resembles the decrease in responsivity during storage of EG&G boron-diffused diodes recently reported by Stock.[10]

V. Conclusion

Perhaps our most general conclusion is that the *n* on *p* photodiodes that we fabricated are inherently more stable than the boron-diffused devices in the UV and blue spectral regions despite equal care in the processing of all diode types. We attribute this to a combination of factors. First, we believe that the Si–SiO_2 interface is rather fragile, and that it is difficult both to

eliminate recombination states there, and to prevent them from forming due to various forms of environmentally induced stress. Second, the presence in the n on p devices of a built-in field near the oxide–silicon interface (deliberate in the case of the phosphorus-diffused devices, and unavoidable in the case of the inversion layer devices) that minimizes the time that photogenerated minority carriers spend in the vicinity of that interface significantly reduces the sensitivity of the n on p devices to any changes that do occur at the interface during the life of the device.[18,19] Third, and perhaps most important, boron-diffused diodes seem to have an inherent sensitivity to moisture that neither the inversion layer nor phosphorus-diffused devices suffer from. Nevertheless, our results show that stable p on n photodiodes can be fabricated provided that scrupulous attention is given to avoiding metallic impurity contamination during wafer processing, and moisture contamination during monitoring and storage of the devices.

Our second conclusion is that the use of a dry, clean oxide process during the growth of the final antireflection coating is essential to achieve excellent stability against UV exposure. We believe that different mechanisms are involved in the case of the different types of diode, but that the result is the same. In the case of the boron- and phosphorus-diffused devices, it is the high, if not perfect, stability of the interface itself that prevents the loss of UV quantum efficiency. In the case of the inversion layer diodes, it is the stability of the oxide trapped charge, which induces the inversion layer, that prevents the loss of linearity range. Indeed, the processing sequences described above have been adopted for the current UDT DRV series of inversion layer photodiodes, and they pass all the accelerated aging tests described in this paper as shown in the figures. In fact, they show no detectable degradation in quantum efficiency and only marginal loss of linearity range after 60 days at 20 mW/cm^2 of 254-nm radiation. This is in marked contrast to the older inversion layer diodes, which were found to lose linearity after several hours exposure to 60 mW/cm^2 of UV radiation.[36]

We wish to thank Dick Duda for the large body of spectral responsivity data that he has carefully taken in the support of stability studies, of which the data reported here are only a small fraction, Jeanne Houston for the internal quantum efficiency measurements, and one of the authors (R.K.) wishes to thank N. Taneja for continued support during the duration of the project.

References

1. E. F. Zalewski and C. R. Duda, "Silicon Photodiode Device with 100% External Quantum Efficiency," Appl. Opt. **22**, 2867 (1983).
2. L-P. Boivin and F. T. McNeeley, "Electrically Calibrated Absolute Radiometer Suitable for Measurement Automation," Appl. Opt. **25**, 554 (1986).
3. E. Kool, "Influence of Heat Treatment and Ionizing Radiation on the Charge Distribution and Number of Surface States in the Si–SiO_2 System," IEEE Trans. Electron Devices **ED-13**, 238 (1966).
4. M. A. Lind and E. F. Zalewski, "Silicon Photodetector Instabilities in the UV," Appl. Opt. **15**, 1377 (1976).
5. A. R. Schaefer, "Ultraviolet Enhanced Responsivity of Silicon Photodiodes: an Investigation," Appl. Opt. **16**, 1539 (1977).
6. R. L. Booker and J. Geist, "Photodiode Quantum Efficiency Enhancement at 365 nm: Optical and Electrical," Appl. Opt. **21**, 3987 (1982).
7. W. Budde, *Optical Radiation Measurements. Vol. 4: Physical Detectors of Optical Radiation* (Academic, New York, 1983), p. 244.
8. J. L. Gardner and F. J. Wilkinson, "Response Time and Linearity of Inversion Layer Silicon Photodiodes," Appl. Opt. **24**, 1531 (1985).
9. K. D. Stock and R. Heine, "On the Aging of Photovoltaic Cells," Optik **71**, 137 (1985).
10. K. D. Stock, "Temporal Stability of Silicon Photodiodes," in *Proceedings, Twelfth International Symposium of Technical Communications on Photon Detectors*, Varna, Sept. 1986 (IMEKO Secretariat H-1371, Budapest POB, 457), p. 129.
11. E. F. Zalewski, "Recent Developments in the Techniques for the Self-Calibration of Si Photodiodes," in *Proceedings, Tenth International Symposium of Technical Communications on Photon Detectors*, Berlin, Sept. 1982 (IMEKO Secretariat H-1371, Budapest POB, 457), p. 127.
12. P. J. Key, N. P. Fox, and M. L. Rastello, "Oxide-Bias Measurements in Silicon Photodiode Self-Calibration Technique," Metrologia **21**, 18 (1985).
13. J. Verdebout and R. L. Booker, "Degradation of Native Oxide Passivated Silicon Photodiodes by Repeated Oxide Bias," J. Appl. Phys. **55**, 406 (1984).
14. J. Verdebout, "Semiquantitative Model for the Oxide Bias Experiment and Its Application to the Study of p^+nn^+ Photodiode Degradation," Appl. Opt. **23**, 4339 (1984).
15. J. Geist, "Silicon Photodiode Front Region Quantum Efficiency Models," J. Appl. Phys. **51**, 3993 (1980).
16. E. F. Zalewski and J. Geist, "Silicon Photodiode Absolute Spectral Response Self-Calibration," Appl. Opt. **18**, 1214 (1980).
17. T. Hansen, "Silicon UV-Photodiode Using Natural Inversion Layers," Phys. Scr. **18**, 471 (1978).
18. J. Geist, E. Liang, and A. R. Schaefer, "Complete Collection of Minority Carriers from the Inversion Layer in Induced Junction Diodes," J. Appl. Phys. **52**, 4879 (1981).
19. R. Korde and J. Geist, "Stable, High Quantum Efficiency Silicon Photodiodes by Arsenic Diffusion," Solid State Electron. **30**, 89 (1987).
20. R. Korde, "Induced Metallurgical Junction UV-Enhanced Silicon Photodiodes," in *Proceedings, First International Conference on Silicon Materials and Technology*, Abstract (Oregon State U., Portland, 1985).
21. V. G. Weizer *et al.*, "Photon Degradation Effects in Terrestrial Silicon Solar Cells," J. Appl. Phys. **50**, 4443 (1979).
22. L. Manchandra, "Hot Electron Trapping Generic Reliability of p^+ Polysilicon/SiO_2/Silicon Structures for Fine Line CMOS Technology," in 24th Annual *Proceedings, Twenty-Fourth Annual Conference on Reliability Physics* (IEEE, New York, 1986), p. 183.
23. A. J. Tavendale and A. A. Williams, "Hydrogen Injection and Neutralization of Boron Acceptors Boiled in Water," Appl. Phys. Lett. **48**, 590 (1986).
24. K. Hofmann and M. Schultz, "Effect of Processing on Interface and Silicon Bulk Traps in MOS Structures," in *Insulating Films on Semiconductors*, J. J. Simonne and J. Buxo, Eds. (North-Holland, New York, 1986), p. 173.
25. V. Zekeria and T. Ma, "Dependence of Radiation-Induced Interface Traps on Gate Electrode Material in Metal/SiO_2/Si Devices," Appl. Phys. Lett. **47**, 54 (1985), and references therein.
26. K. Blumenstock and R. Hezel, "Interface State Generation in the Si–SiO_2 System by Non-Ionizing UV Irradiation," in *Insu-*

lating Films on Semiconductors, J. J. Simonne and J. Buxo (North-Holland, New York, 1986), p. 221.
27. R. Korde, unpublished.
28. J. F. Naber and F. K. Hopkins, "Edge Illumination of a Silicon Photodiode at Ultraviolet Wavelengths," Appl. Opt. **26,** 21 (1987).
29. J. Geist and E. F. Zalewski, "The Quantum Yields of Silicon in the Visible," Appl. Phys. Lett. **35,** 503 (1979).
30. J. Geist, E. F. Zalewski, and A. R. Schaefer, "Spectral Response Self-Calibration and Interpolation of Silicon Photodiodes," Appl. Opt. **19,** 3795 (1980).
31. S. K. Ghandhi, *VLSI Fabrication Principles: Silicon and Gallium Arsenic* (Wiley, New York, 1983), p. 163.
32. C. M. Botchek, *VLSI Basic MOS Engineering, Vol. 1* (Pacific Technical Group, Inc., Sarasota, CA, 1984), p. 275.
33. Z. A. Weinberg *et al.*, "Reduction of Electron and Hole Trapping in SiO_2 by Rapid Thermal Annealing," Appl. Phys. Lett. **45,** 1204 (1984).
34. Reference in this paper to commercial products is provided to adequately described the experimental technique. It implies neither endorsement by the National Bureau of Standards nor that the product so referenced is the best for the purpose.
35. S. Armstrong, Epoxy Technology, Billerica, MA; personal communication.
36. A. D. Wilson and H. Lyall, "Design of an Ultraviolet Radiometer. 2. Detector Optical Characteristics," Appl. Opt. **25,** 4530 (1986).
37. J. Geist and C. S. Wang, "New Calculations of the Quantum Efficiency of Silicon in the Near Ultraviolet," Phys. Rev. B **27,** 4841 (1983).

Patter *continued from page 5283*

reached by normal spraying techniques. Coverage by the system is expected to be more complete than that obtained by hand brushing. The applicator is held by hand-pressure against the surface holding the object to be painted (see Fig. 11). A rubber seal contains the painting atmosphere and prevents the unwanted spread of paint out of the area to be coated. A locating pin is extended to a matching hole in the object to be coated to assure the correct positioning of the applicator.

The painting sequence includes application, reapplication, and venting intervals. During the application interval, paint is atomized and fed into the inner chamber. The residual atomized paint flows under the end of the inner chamber to the outer chamber. The volume of residual atomized paint is controlled by the paint pressure in the atomizer and the size of the expansion tank connected to the outer chamber. Regulators and valves could also be used to duplicate the function of the expansion tank. The reapplication interval begins with the evacuation of the inner chamber. This causes the atomized paint to flow back from the outer chamber to the inner chamber, coating surfaces that were not reached during the application interval. In addition, the evacuation might be halted and resumed once or several times in a controlled manner to create pressure/vacuum pulses that would alternately accelerate and decelerate the flow of atomized paint toward the fastener. During the venting interval, the inner chamber is evacuated more completely. The remaining paint and air in the secondary chamber is withdrawn into the primary chamber and the check valve opens, allowing air to be drawn into the expansion tank and outer chamber. Thus, the atomized paint is flushed from the chambers, and excess paint is removed from the fastener.

An alternative version (see inset in figure) relies on electrostatic attraction to apply the paint to the fastener. In this case, the inner tube serves as a positive electrode and the fastener as the negative electrode. An insulator on the inside of the inner tube prevents accidental electrical contact between the two electrodes. Voltage regulators and electronic sensors help to guard against arcing.

This work was done by J. Arthur Leifsen of Grumman Aerospace Corp. for Johnson Space Center. Refer to MSC-21080.

Slot-height measuring system

A measuring system that includes a slot-depth transducer and a wheel-driven rotary optical encoder makes repeated measurements of slot depth vs position along the slots on the leading and trailing edges of the blown rotor blades of an experimental aircraft. An x-y recorder plots the slot depth and position on 28- by 43-cm paper so that the measurements can be studied visually to monitor progress in the rotor-tuning process. The moving parts of the measuring system (see Fig. 12) include a carriage that supports the slot-depth transducer and the wheel with the encoder. The transducer and encoder are both commercially available components. The carriage

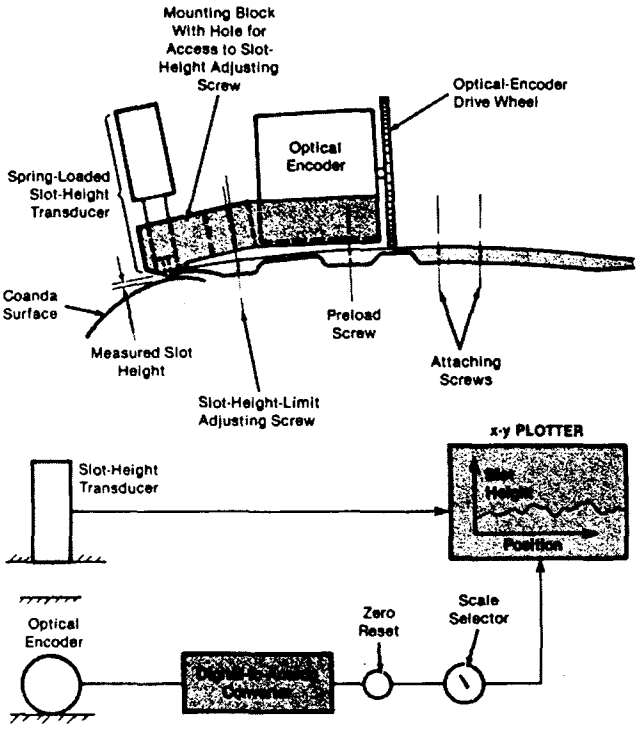

Fig. 12. Slot-depth measuring system uses a spring-loaded transducer to measure the slot depth and a wheel-driven rotary optical encoder to measure the position along the slot. An x-y recorder plots the depth vs the position.

uses the upper surface and edge of the rotor slot as guides and reference points.

The slot-height transducer is a spring-loaded unit with a range of 2.5 mm and a sensitivity of 0.025 mm; the transducer output drives the y-axis input of the recorder. The output of the rotary optical encoder gives the relative spanwise location of the measuring unit as the wheel rolls along the rotor blade. The encoder output is passed through a digital-to-analog converter, the output of which drives the x axis of the recorder. The plotter controls include an automatic reset-to-zero switch on the position input so that a slot-height scan can be started at any location along the rotor slot and from any encoder position. A range switch for the position input allows the full plotter paper length to be used for various blade spans; for example, 1.5, 3, or 9 m. The y-axis plotter scale is 1 unit for each 0.01 unit of slot height. The cost of the system is estimated to be less than $10,000.

continued on page 5298